



Occurrence of Local Tsunamis Along the Eastern Coast of the Korean Peninsula Based on Numerical Modeling of Historical Earthquakes

Taemin Ha¹, Jae-Seon Yoon², Jai Bok Kyung³, Seok-Hoon Yoon⁴, Dong-Woo Lee¹ and Kwang-Hee Kim^{5*}

¹Department of Civil Engineering, Kangwon National University, Samcheok, South Korea, ²Rural Research Institute, Korea Rural Community Corporation, Ansan, South Korea, ³Department of Earth Science Education, Korea National University of Education, Cheongju, South Korea, ⁴Department of Earth and Marine Sciences, Jeju National University, Jeju, South Korea, ⁵Department of Geological Sciences, Pusan National University, Busan, South Korea

OPEN ACCESS

Edited by:

Gang Rao,
Southwest Petroleum University,
China

Reviewed by:

Kenji Satake,
The University of Tokyo, Japan
Jörn Behrens,
Universität Hamburg, Germany

*Correspondence:

Kwang-Hee Kim
kwanghee@pusan.ac.kr

Specialty section:

This article was submitted to
Geohazards and Georisks,
a section of the journal
Frontiers in Earth Science

Received: 16 December 2021

Accepted: 09 May 2022

Published: 27 May 2022

Citation:

Ha T, Yoon J-S, Kyung JB, Yoon S-H,
Lee D-W and Kim K-H (2022)
Occurrence of Local Tsunamis Along
the Eastern Coast of the Korean
Peninsula Based on Numerical
Modeling of Historical Earthquakes.
Front. Earth Sci. 10:836168.
doi: 10.3389/feart.2022.836168

Korean historical literature records a major offshore earthquake with an associated tsunami in the East Sea of Korea in 1681. The event also generated strong ground motion and landslides over the Korean Peninsula. This study examined the occurrence and characteristics of the reported tsunami along the eastern coast of the peninsula using numerical modeling of tsunami propagation from submarine faults identified in a recently compiled marine fault map. Results from some scenarios indicated runup heights in good agreement with descriptions in historical records. We also examined the time required for tsunamis to travel from the causative faults to vulnerable areas along the eastern coast under various scenarios. Our results successfully hindcast the occurrence and effects of local tsunamis in the historical literature and have important implications for assessing tsunami hazard and risk for coastal areas of the Korean Peninsula.

Keywords: historic tsunami, numerical model, fault parameter, local tsunami, runup height

1 INTRODUCTION

The duration of an earthquake spans only a few seconds or minutes, but the direct or indirect human, material, economic, and social damage caused by earthquakes can be significant. However, when accompanied by a tsunami, the scope and magnitude of damage may increase dramatically, posing a considerable threat to human lives and infrastructure. Large earthquakes occur mostly at plate boundaries and cause significant casualties and infrastructural/property damage. However, large destructive earthquakes also occur inside plates, as observed during the 1976 Tangshan, China, earthquake (e.g., Butler et al., 1979) and the 1811–1812 New Madrid earthquakes in the central United States (e.g., Johnston and Schweig, 1996).

Historical earthquakes and tsunamis in Korea are well documented in various historical records. For example, two major earthquakes and tsunamis, which occurred in 1643 and 1681 in the East Sea of Korea, are recorded in the Annals of the Joseon Dynasty (Kyung et al., 2010). Earthquakes in the instrumental observation period since 1905 in Korea have occurred sporadically over a wide area both on land and offshore (KMA, 2022). Recent earthquakes with a local magnitude (M_L) of 5.8 in Gyeongju and M_L 5.4 in Pohang caused substantial damage in the epicentral areas (Kim et al., 2016; Ministry of Public Safety and Security, 2017; Kim et al., 2018a, b; Ministry of the Interior and Safety, 2018). In addition, although not damaging, large earthquakes with a magnitude of >5 have occurred

frequently in the eastern offshore area of the Korean Peninsula, including two M_S (surface wave magnitude) 6.0 earthquakes in 1963, an M_L 5.2 earthquake in 1999, an M_L 5.2 earthquake in 2004, and most recently an M_L 5.0 earthquake in 2016 (ISC, 2022; KMA, 2022). Consequently, an understanding of earthquakes, faults and tsunamis is considered paramount in better understanding the nature of coastal hazards in Korea (Chiu and Kim, 2004; Lee and Yang, 2006; Kyung et al., 2010).

Frequent large earthquakes are presumed to occur by the reactivation of submarine faults that formed during the opening of the East Sea during the late Oligocene to early Miocene. It is also suspected that faults potentially hosting large earthquakes exist in regions where the transition from oceanic to continental crust occurs (Kim, 1982). Although it is necessary to monitor offshore earthquakes in the East Sea and characterize them to understand their hazards and risks, this monitoring is challenging compared with continental earthquakes.

This study examined the records of earthquakes and tsunamis in the East Sea of Korea that are recorded in historical literature. These historical earthquakes are presumed to have been centered in the eastern offshore of the Korean Peninsula and generated local tsunamis without widespread triggering. We identified 15 potential faults after carefully reviewing historical records of earthquakes, as well as modern marine seismic information and generated 15 scenarios (corresponding to the 15 identified faults) for numerical tsunami modeling. We then compare the results with tsunami records in the historical literature and discuss the potential for and risks of local tsunami occurrences in the East Sea.

2 DATA AND METHODOLOGY

Historical earthquake reports, including for more than 470 events with a modified Mercalli intensity (MMI) of greater than or equal to V, are available for the period between AD 2 and AD 1904 (e.g., Lee and Yang, 2006; Kyung et al., 2010). Reports of a series of earthquakes in June 1681 are particularly interesting, as the series shows a typical foreshock–mainshock–aftershock sequence. The historical records also mention a small-scale tsunami. Felt and damage reports were made throughout the Korean Peninsula. To gain an appreciation for the type of information available concerning the 1681 earthquake and tsunami, consider the following descriptions contained in the Diaries of the Royal Secretariat:

Residences were shaken, and windows were rattled. People ran in fear, and trees were also shaken. . . . Three aftershocks occurred in 1 day. . . . Stone fences collapsed, and roof tiles were displaced. Some rocks were split by the force. . . . The coastal line changed as if the tide had gone out. It was an extraordinary event.

The historical events are usually reported in historical literature but their descriptions are only anecdotal and qualitative in nature, although are sufficiently clear to be

interpreted in terms of the occurrence and behavior of a tsunami:

There were earthquakes reported in several areas of Gangwon province followed by thunderous sound, and a strange collapse of the rocky cliff in Doota Mountain was witnessed. Broken boulders up to 30 m were observed in the sea, and the coast shaped as a receding tide, but where water was full on a regular day was around 100 steps or 5–60 steps exposed at several beaches located in the Samcheok area.

When a large tsunami approaches the coast, a strong backwash is commonly observed on the coast because of the conservation of mass. It is thought that the historical literature quoted above described the strong backwash of a tsunami. Therefore, in this study, the local tsunami event that occurred in 1681 was selected for study, as the event recorded the maximum intensity reported in historical documents and contained the most detailed description of a tsunami-like phenomenon in the Diaries of the Royal Secretariat. The occurrence of this event was validated (see **Section 3.2**). **Figure 1** shows the approximate location of the 1681 earthquake epicenter (red star) and areas of felt reports (red dots), as reported by the Diaries of the Royal Secretariat.

2.1 Fault Scenarios

For studies of earthquakes and tsunamis, the timing, location, and size of the event are essential data. In the recent compilation of Kyung et al. (2010), epicenters, magnitudes, and intensities were estimated on the basis of descriptions and felt areas in the historical literature. Those authors estimated the magnitude of the largest event in the sequence as a local magnitude 6.7 with $MMI = VIII-IX$, with the epicenter located offshore between Yangyang and Samcheok (37.9°N, 120.1°E).

We reviewed the available marine geological fault databases and selected significant faults to assess the potential for tsunamis in the East Sea. During the review, we considered instrumental records of seismicity available from the Korea Meteorological Administration (KMA, 2022), the International Seismological Centre (ISC, 2022), and published papers (e.g., Park and Mori, 2005; Kim et al., 2016; Han et al., 2019; Park et al., 2020); the high-resolution bathymetry map published by the Korea Hydrographic and Oceanographic Agency (KIGAM, 2016); an inventory of submarine landslides compiled by Yoon et al. (2015); and faults identified from marine seismic data (Schulter and Chun, 1974; KIGAM, 2010). We also reviewed sedimentological and stratigraphic studies to help estimate recent fault activity (Yoon, 1994; Yoo et al., 2019).

Locations of faults and corresponding fault parameters generating the maximum initial surface displacement were identified from the integrated database of the recently revised geological structural map of the area around the East Sea continental margin (KIGAM, 2016). Then, tsunami scenarios were improved by changing the fault parameters (**Figure 2**), including introduced earthquake magnitude and fault

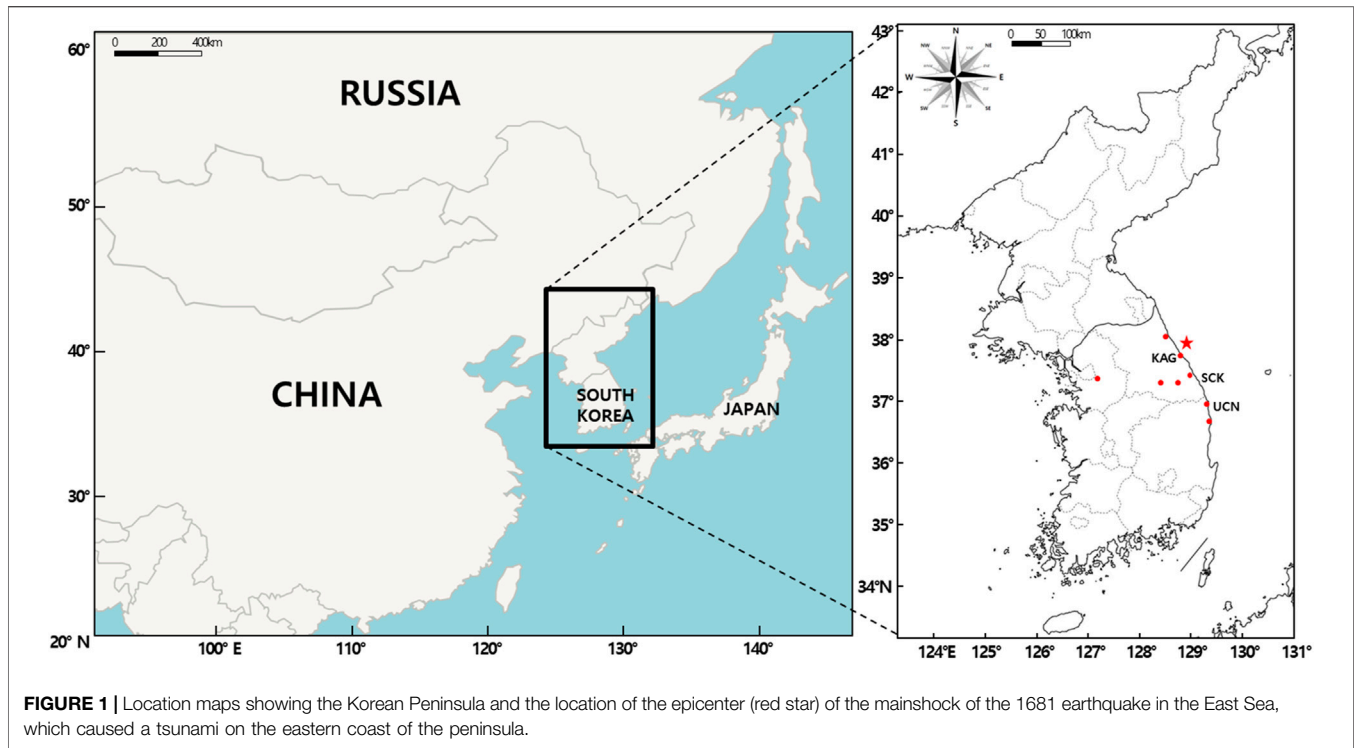


FIGURE 1 | Location maps showing the Korean Peninsula and the location of the epicenter (red star) of the mainshock of the 1681 earthquake in the East Sea, which caused a tsunami on the eastern coast of the peninsula.

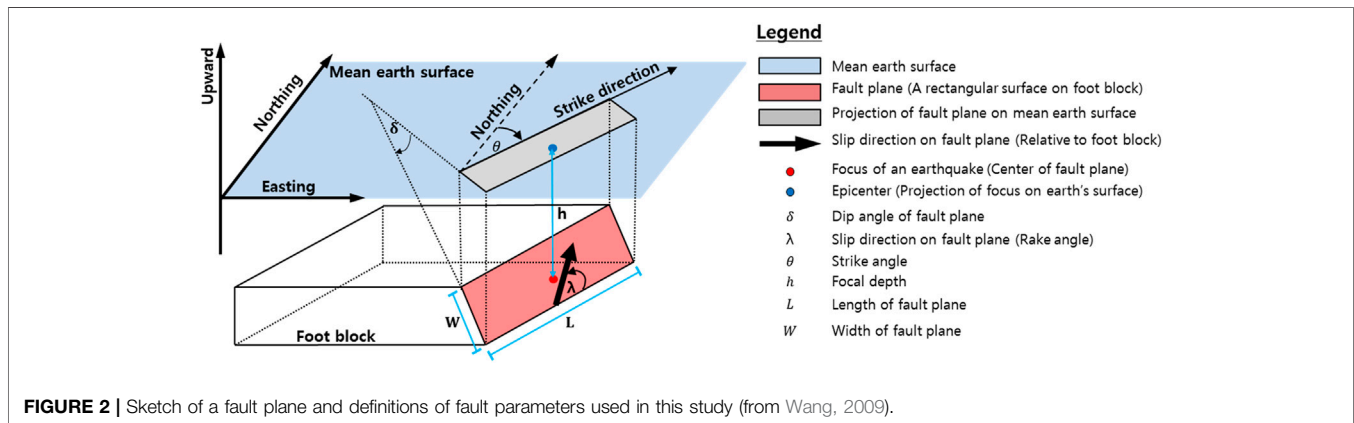


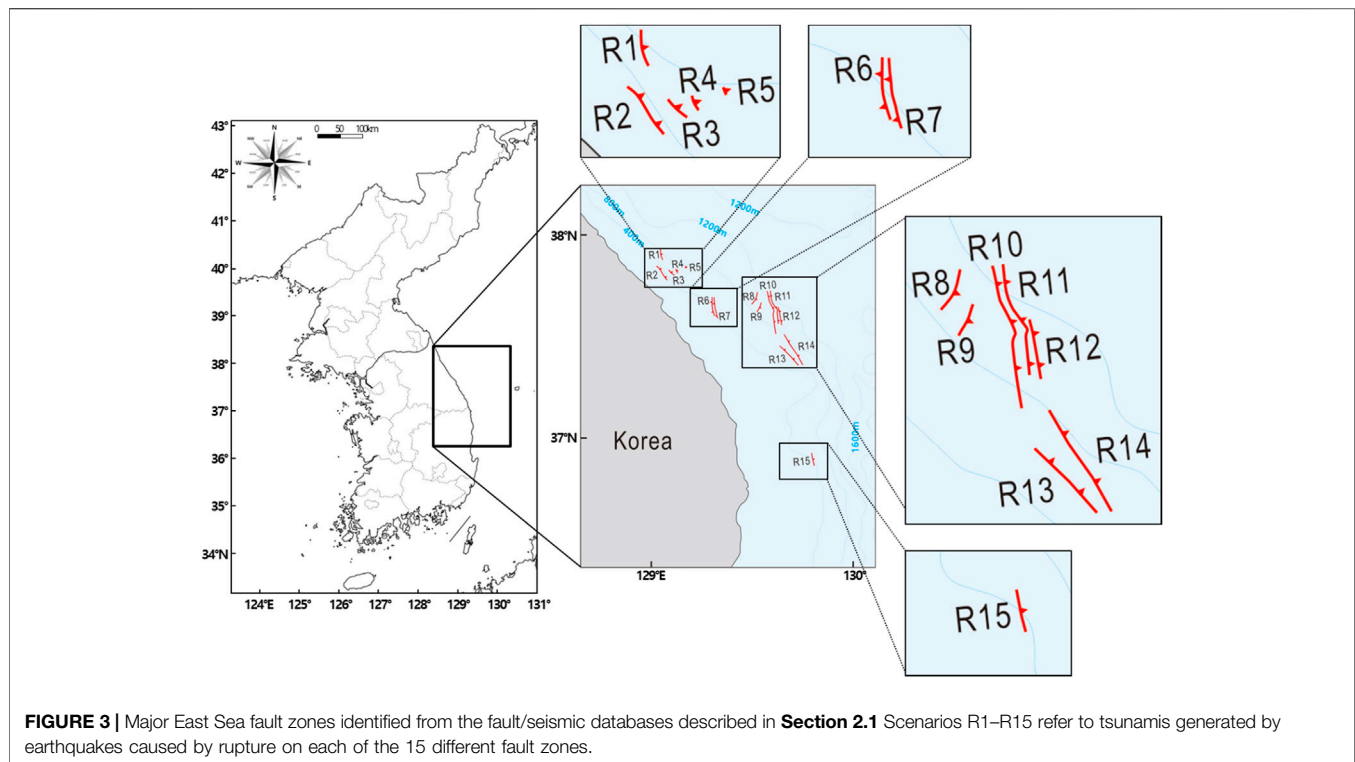
FIGURE 2 | Sketch of a fault plane and definitions of fault parameters used in this study (from Wang, 2009).

displacement. In addition, tsunami impact was examined *via* the formation of the initial sea surface displacement according to the fault-parameter scenario and numerical modeling of tsunamis.

Our review of recently compiled marine fault databases and related studies identified 15 faults potentially responsible for major earthquakes or discontinuities in marine seismic data in the eastern offshore of the Korean Peninsula (Figure 3). For those faults, we assigned fault parameters for tsunami scenarios. Each fault scenario consisted of earthquake magnitude and vertical displacements, estimated on the basis of empirical equations (Figure 2 and Table 1; Matsuda, 1975; Bonilla et al., 1984; Wells and Coppersmith, 1994; Anderson, 1996; Vakov, 1996). Although there are large uncertainties, we assumed a fault dip of 90° .

2.2 Calculation of the Initial Sea Surface Displacement Based on Fault-Parameter Scenarios

In this study, the COMCOT v1.7 (Wang, 2009) was used for tsunami modeling and the Okada model (Okada, 1985) included in the COMCOT v1.7 was applied to generate the initial sea surface displacement. The Okada model has been utilized in tsunami-related research fields for calculating the initial sea surface displacement of tsunamis generated by submarine earthquakes. This model can be applied to a variety of fields, as it is fully validated in quantitative and qualitative aspects (Son et al., 2011; Wang and Liu, 2011; Lynett P. J. et al., 2012; Wijetunge, 2012; Chai et al., 2014; Ha and Cho, 2015; Kim K.



H. et al., 2018; Lee E. et al., 2019). In this study, the initial sea surface displacement were generated according to each fault-parameter scenario mentioned above in **Section 2.1**. As the sizes of the initial sea surface displacement calculated for scenarios R03 to R05 and R08 to R09 were very small and the maximum wave heights less than 0.1 m, those five scenarios were excluded from the analysis of tsunami impact. Scenario R01 showed a maximum wave height of >0.1 m, but the location of the generated tsunami was similar to the location of occurrence of scenario R02, resulting in the additional exclusion of scenario R01 from the analysis. As a result, the tsunamis of nine scenarios were generated, for which the initial sea surface displacement are illustrated in **Figure 4**.

The initial sea surface displacement manifested differently according to variation in fault parameters. The major propagation directions of the tsunami were varied according to the fault plane strike angle. The tsunami source area was presumed to be proportional to fault length and width. In general, the maximum runup height of tsunamis is the most critical variable in tsunami hazard assessments on the coast. Of the fault parameters, the maximum wave height calculated through tsunami modeling is quantitatively most closely related to the maximum displacement of the initial sea surface displacement. The maximum displacement of the initial tsunami wave in this study was calculated according to the extent of fault plane displacement and the upper fault plane depth, for which an initial tsunami wave with less than 0.5 m maximum displacement was generated in most scenarios. However, a large tsunami with a maximum displacement of >0.5 m was generated in a few scenarios, such as R10, R11, and R14,

considered as presenting high tsunami potentials and related risks. In particular, large tsunamis that exceeded a maximum displacement of 1.5 m were generated in some scenarios. The maximum value was adopted for the dip angle of the fault plane so that the maximum displacement would be generated. When the absolute size of the tsunami calculated according to the maximum value decreased, the initial sea surface displacement of the tsunami was recalculated by appropriately combining the middle and lowest values so that the maximum value was yielded. Quantitative verification was difficult for the generated initial sea surface displacement because no previous data were observed for comparison. Therefore, the initial tsunami wave deformation according to variation in fault parameters was analyzed qualitatively. It was determined that the initial sea surface displacement changed fairly consistently with respect to fault parameter modifications, despite the seafloor topography and water depth of the fault zones being unique for all examined regions.

2.3 Configuration of Numerical Modeling and the High-Resolution Grid System of the East Sea

A high-resolution digital bathymetric model of the East Sea for numerical modeling of tsunami propagation was generated using numerical topographic data obtained from the KMA (**Figure 5**) so that the digital bathymetric model can be linked with the existing KMA database (Park et al., 2020). Thus, the maximum wave heights of tsunamis calculated using the scenarios can be added to the national disaster prevention plan for tsunami hazard

TABLE 1 | Fault parameter scenarios corresponding to the major East Sea fault zones. The definitions of these parameters are referred to **Figure 2**.

Fault name	Seismic sections	Longitude (°E)	Latitude (°N)	H (km)	θ (°)	λ (°)	L (km)	W (km) CombA	W (km) CombB	D (km) CombA	D (km) CombB	δ (°)			
												Top	Middle	Bottom	Mean
R1	02GH-08, 09	129.046 129.057	37.931 37.878	1.3	355.0	90.0	5.71	2.8	2.85	0.285	0.216	74.6 (165–826 m)	55.6 (826–1487 m)	40.1 (1487–2148 m)	56.8
R2	00AD-8, 9	129.025 129.080	37.847 37.769	0.5	330.0	90.0	9.30	2.9	4.65	0.530	0.400	58.6 (57–622 m)	42.8 (622–1187 m)	30.7 (1186–1752 m)	44.0
R3	00AD-8, 02GH-07A	129.085 129.114	37.829 37.802	0.8	320.0	90.0	4.10	3.6	2.05	0.205	0.150	44.6 (74–652 m)	26.0 (652–1230 m)	18.9 (1230–1808 m)	29.8
R4	00AD-8, 02GH-07A	129.121 129.131	37.834 37.812	0.9	343.0	90.0	2.50	1.6	1.25	0.130	0.090	83.8 (73–602 m)	57.3 (602–1131 m)	37.5 (1131–1660 m)	59.5
R5	00AD-8, 02GH-07A	129.168 129.172	37.846 37.835	1.3	345.0	90.0	1.28	1.7	0.64	0.080	0.048	76.3 (200–623 m)	49.7 (623–1046 m)	28.5 (1046–1469 m)	51.5
R6	00AD-5, 11, 02GH-03, 04	129.301 129.313	37.694 37.601	0.6	358.0	90.0	9.78	2.5	4.89	0.575	0.432	80.9 (56–926 m)	63.5 (926–1796 m)	47.8 (1796–2666 m)	64.1
R7	00AD-5, 02GH-03, 04	129.311 129.329	37.693 37.589	0.8	356.0	90.0	11.11	2.3	5.56	0.715	0.528	77.5 (32–827 m)	56.7 (827–1622 m)	46.6 (1622–2417 m)	60.3
R8	02GH-03, 04, 14	129.526 129.497	37.719 37.659	1.4	33.0	90.0	6.95	2.5	3.48	0.355	0.272	74.9 (39–559 m)	39.8 (559–1079 m)	22.2 (1079–1599 m)	45.6
R9	02GH-03, 14	129.545 129.523	37.667 37.620	1.3	31.0	90.0	5.38	2.4	2.69	0.265	0.202	66.4 (31–587 m)	34.5 (587–1143 m)	23.1 (1143–1699 m)	41.3
R10	00AD-02, 03, 04, 02GH-01, 02, 03, 04	129.573 129.617	37.724 37.513	1.3	355.0	90.0	22.57	2.6	11.28	3.025	1.856	57.9 (94–683 m)	34.2 (683–1272 m)	20.8 (1272–1861 m)	37.6
R11	00AD-03, 04, 02GH-01, 02, 03, 04	129.589 129.629	37.727 37.563	1.5	353.0	90.0	17.67	1.9	8.83	1.730	1.146	58.2 (51–499 m)	43.7 (499–947 m)	29.4 (947–1395 m)	43.8
R12	00AD-03, 02GH-01, 02	129.629 129.645	37.635 37.557	1.4	356.0	90.0	9.42	1.6	4.71	0.540	0.410	64.0 (94–542 m)	43.2 (542–990 m)	31.8 (990–1438 m)	46.3
R13	01GH-11, 12, 13	129.636 129.729	37.454 37.359	0.9	323.0	90.0	13.90	0.7	6.95	1.045	0.740	71.0 (134–400 m)	36.7 (400–666 m)	21.8 (666–932 m)	43.2
R14	01GH-11, 12, 13, 14	129.658 129.740	37.511 37.361	1.1	335.0	90.0	18.45	1.2	9.23	1.880	1.230	54.1 (64–335 m)	31.9 (335–606 m)	22.7 (606–877 m)	36.2
R15	05GH-36, 38, 01GH-02	129.794 129.808	36.927 36.864	0.9	354.0	90.0	11.28	0.8	5.64	0.740	0.546	88.1 (61–278 m)	86.1 (278–495 m)	79.3 (495–712 m)	84.5

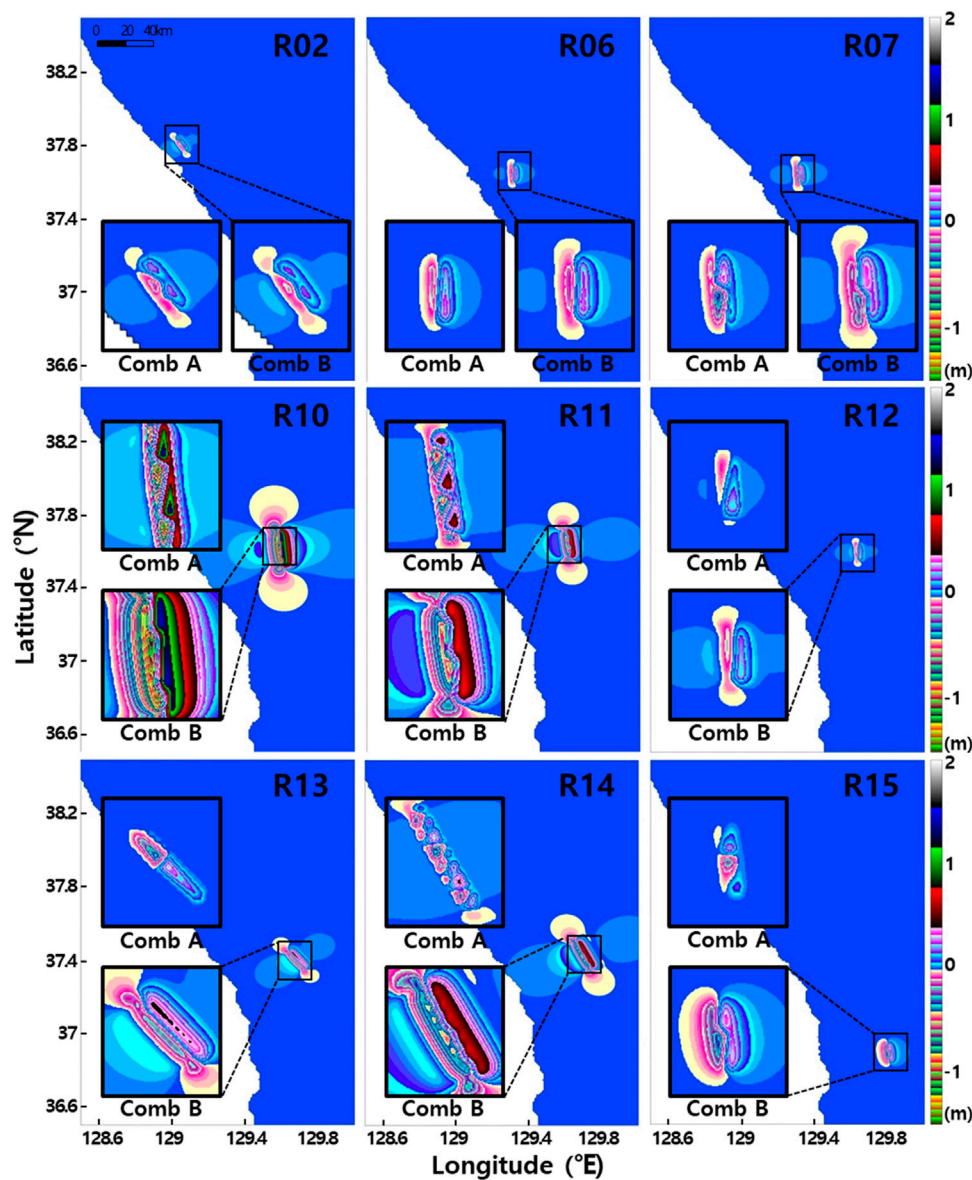
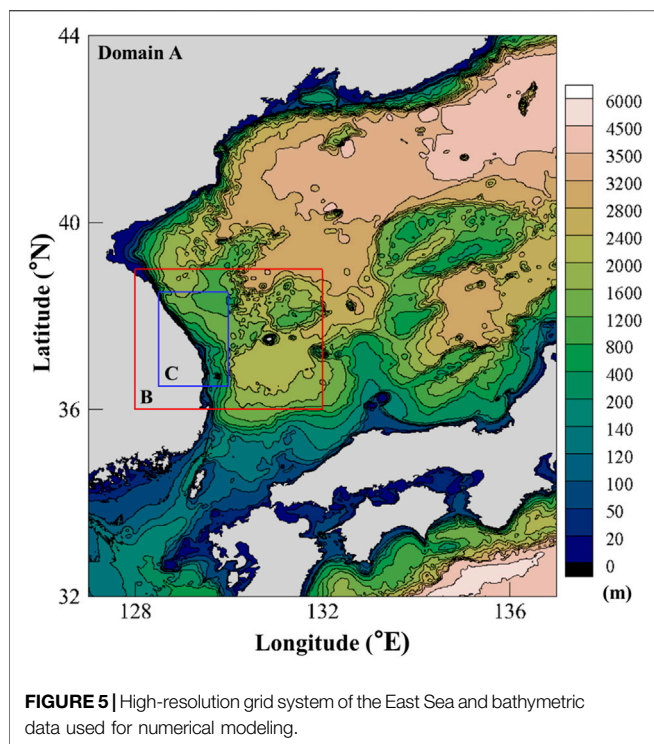


FIGURE 4 | The initial sea surface displacement according to variations in fault parameters (see **Section 2.2** for details). “Comb” is “combination” (see **Section 3.1** for details). “R” refers to scenario (fault zone) number.

in conjunction with the existing tsunami database (Lee et al., 2019b; Park et al., 2020). This wave-height information could also be used to forecast a possible future tsunami if used together with existing data. This study aimed to assess the potential of occurrence of local tsunamis in the East Sea. As existing observational data were not based on accurate recordings from on-land areas, the impact of possible local tsunamis was estimated by calculating the tsunami runup height at the coast using Green’s law rather than computing landward inundation in the model directly. Therefore, numerical modeling of tsunami inundation for land areas was not performed in the present study. However, the tsunami wave height increases owing to the shoaling effect caused by the decrease of water depth at the

coast. In such a case, the maximum wave height on the coast can be affected with an increase in the nonlinearity of waves. Therefore, a tsunami inundation model (COMCOT v1.7), which employs a nonlinear shallow-water equation, was applied to calculate the maximum tsunami elevation in the numerical domain near the coast to consider the above-mentioned phenomena.

For deep-marine areas, a tsunami propagation model that employs a linear shallow-water equation was used to simulate tsunami propagation since the nonlinearity of a tsunami wave can be neglected in deep water. In general, the wavelength of a tsunami is usually very long and a tsunami wave can be modeled using the shallow water wave theory even in deep



water. A grid system for tsunami modeling was built by establishing a total of three numerical domains (grid size: $\Delta x = \Delta y = 0.01^\circ - 0.00111^\circ$) within the geographic coordinate system and dividing them into three stages from A to C using the grid-nesting technique. We introduced three different bathymetric data sources to generate gridded data systems: the gridded data ($\Delta x = \Delta y = 0.01^\circ$) held by the KMA for tsunami modeling, the 2021 15 arc-second gridded bathymetric data of GEBCO Compilation Group (2021), and bathymetric data produced by KHOA specifically for the operation of marine numerical models with ~ 150 m horizontal intervals (Yoo et al., 2019). After careful manipulation to match the datum level, the three bathymetric data sources were implemented to establish the high-resolution grid system for tsunami modeling using the Generic Mapping Tools (GMT; Wessel et al., 1998) program. A description of the grid system is presented in **Table 2**.

3 ESTIMATION OF TSUNAMI WAVE HEIGHT AND VERIFICATION OF HISTORICAL TSUNAMI RECORDS ON THE EASTERN COAST OF THE KOREAN PENINSULA

3.1 Estimation of Tsunami Maximum Wave Height Using Local Tsunami Scenarios

Numerical modeling of tsunami propagation was performed to calculate the maximum wave height of tsunamis based on local tsunami scenarios generated for the eastern coast of the Korean Peninsula. First, we generated 15 virtual local tsunamis following the scenarios described in **Section 2.1** and simulated tsunami

propagation along the eastern coast of the Korean Peninsula. The 6 scenarios described in **Section 2.2** were then excluded after thorough investigation of the numerical results since the generated tsunamis barely affected the eastern coast of the Korean Peninsula. The numerical results varied depending on different combinations (**Table 3**) of the empirical equations adopted in the modeling. Of the various combinations, the two combinations with the highest potential of realistic occurrence considering various scenarios of historical tsunami events and the maximum tsunami wave height were selected by assessing the computed tsunami wave heights. These two combinations are as follows:

- ▷ Combination A: the mean value of calculated displacement from the empirical equations proposed by Matsuda (1975) and Wells & Coppersmith (1994) + the added displacement calculated from the value of the maximum slip angle.
- ▷ Combination B: the mean displacement calculated from the five different empirical equations + the added displacement calculated from the upward adjustment following the relationship between fault width and length [W (km) = $0.5 L$ (km)] + the added displacement calculated from the value of the mean slip angle.

Figures 6, 7 present the numerical results of the highest surface elevation of the tsunamis generated according to each scenario constructed with the two combinations above and their propagation in the East Sea. These two figures display the maximum wave heights of proposed local tsunamis, whereas **Figures 8, 9** show the spatial distribution of the lowest surface elevation of the tsunamis. Overall, the maximum wave heights of the tsunamis were distributed over larger areas for the scenarios using Combination B in comparison with those using Combination A. In most scenarios, the tsunami source area were parallel to the eastern coast of the Korean Peninsula, and the maximum and minimum values were developed perpendicular to the coast. The wave heights of the tsunamis gradually increased as the tsunamis propagated toward the coast mostly because of the shoaling effect, and the maximum wave heights were observed near the coast for the scenarios using both combinations. The absolute value of the highest surface elevation was more than two times higher than that of the lowest surface elevation.

Figure 10 shows the maximum wave heights of the tsunamis generated on the eastern coast of the Korean Peninsula. As some scenarios generated relatively low wave heights less than 0.1 m and were similar in the location of occurrence compared with other fault parameter scenarios as described above in **Section 2.2**,

TABLE 2 | Description of the East Sea high-resolution grid system used in the present study.

Domain	Grid system	Grid size (')	Time step (s)
A	1,001 × 1,201	0.01000	3.00000
B	1,201 × 1,901	0.00333	1.00000
C	1,351 × 1,801	0.00111	0.33333

TABLE 3 | Estimation of the maximum displacement of the fault plane (m) calculated according to various combinations of empirical equations (R: reverse type only, All: reverse type + strike-slip type + normal type).

Fault name	Magnitude (Mean)	Matsuda (1975)	Stemmons (1988, R)	Bonilla et al. (1984, All)	Wells and Coppersmith (1994, R)	Wells and Coppersmith (1994, All)	Maximum displacement (mean)
R1	6.10	0.46	0.29	0.06	0.11	0.16	0.216
R2	6.35	0.65	0.46	0.13	0.41	0.35	0.400
R3	5.93	0.36	0.22	0.03	0.05	0.09	0.150
R4	5.67	0.25	0.14	0.01	0.01	0.04	0.090
R5	5.32	0.16	0.07	0.00	0.00	0.01	0.048
R6	6.38	0.67	0.48	0.15	0.48	0.38	0.432
R7	6.45	0.74	0.55	0.19	0.69	0.47	0.528
R8	6.20	0.52	0.35	0.08	0.19	0.22	0.272
R9	6.07	0.44	0.28	0.05	0.09	0.15	0.202
R10	6.82	1.24	1.05	0.68	4.81	1.50	1.856
R11	6.69	1.03	0.83	0.44	2.43	1.00	1.146
R12	6.36	0.65	0.47	0.14	0.43	0.36	0.410
R13	6.56	0.86	0.66	0.28	1.23	0.67	0.740
R14	6.71	1.06	0.86	0.47	2.70	1.06	1.230
R15	6.46	0.75	0.56	0.20	0.73	0.49	0.546

6 of the 15 scenarios were excluded from the comparison of maximum wave heights of the tsunamis. A higher maximum wave height was observed for Combination B relative to Combination A, noting that the maximum fault displacement was used in Combination A, whereas the mean value was used in Combination B. It was thought that despite using the mean fault displacement in Combination B, the tsunami energy was higher than for the maximum fault displacement owing to the greater size of the fault zone used for this combination and therefore resulted in higher wave heights of tsunamis on the coast. Maximum wave heights of <0.1 m were calculated for fault parameter scenarios with relatively small fault zone sizes, indicating that the impacts of these tsunamis on the coast were insubstantial for these scenarios. In contrast, the maximum wave heights increased as the size of the fault zone increased, and the most significant impact across the studied coastal area was observed for the R10 scenario, in which the size of the fault zone was the largest of the 15 scenarios.

3.2 Comparison and Verification of Tsunami Records in the Diaries of the Royal Secretariat

Slopes of the major beaches located on the studied part of the eastern coast of the Korean Peninsula, such as Gangneung and Samcheok beaches, are quite shallow less than 0.05. The natural beach widths of those areas are approximately 100–200 m, whereas their highest points are located 5–10 m above mean sea level. The Diaries of the Royal Secretariat described the tsunami as “shaped as a receding tide, but where water was full on a regular day was around 100 steps or 5–60 steps exposed.” Here, 100 steps converted to the SI unit system measures about 150 m, which is similar to natural beach widths along the studied coastline. The phenomenon described in the historical text is considered to be similar to a tsunami rundown, in which coastal waters recede and then amplify the wave height of a tsunami that approached nearshore before the tsunami runup. The runup

phenomenon following the rundown exhibits similar wave heights to those of numerical results, with runup heights of 5–10 m along the beach slope. Numerical modeling for the tsunami scenarios suggests that a maximum runup height occurrence of 5–10 m in the location described in the Diaries of the Royal Secretariat is plausible (Figures 10, 11). Furthermore, the damage caused by a local tsunami as described in historical tsunami records is also plausible considering the maximum runup heights as possible. Although the verification is qualitative in nature, the numerical modeling results based on tsunami scenarios in combination with tsunami records in the Diaries of the Royal Secretariat indicate that there is a risk of local tsunamis on the eastern coastline of the Korean Peninsula.

4 POTENTIAL FOR LOCAL TSUNAMI GENERATION IN THE EAST SEA

4.1 Tsunami Propagation in the East Sea and Arrival Time to the Coastline From the Source

The initial sea surface displacement were modeled according to each tsunami scenario, following which tsunami propagation through the East Sea was modeled to calculate the propagation distance and arrival time of the tsunami (Figure 12).

As seen in Figure 12, tsunamis are generated at a distance of 10–50 km from the eastern coast of the Korean Peninsula and reach the East Sea coast between 5 and 20 min after initiation. The current tsunami forecasting system in South Korea is capable of handling local tsunamis around the Korean Peninsula based on the tsunami elevation database established by KMA. Although local tsunamis are routinely computed in the database, their impact on the eastern coast has not been thoroughly studied. In contrast, tsunami-related forecasts in Japan are executed within 3 minutes after an earthquake and include various local

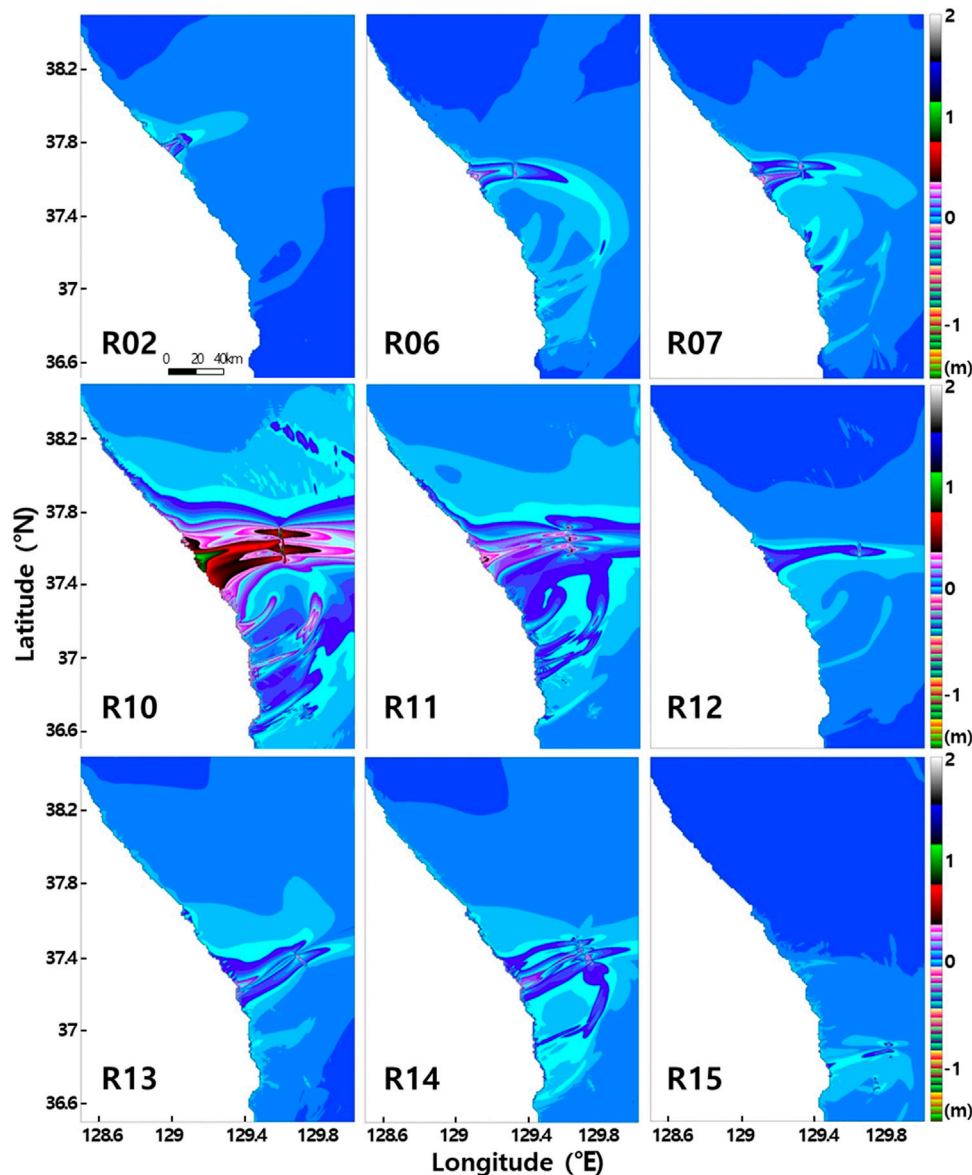


FIGURE 6 | Maximum wave height of tsunamis in the East Sea, estimated from numerical modeling for different scenarios (fault zones; Combination A).

tsunami scenarios. A rapid warning system for forecasting local tsunamis has not been established in South Korea's national tsunami disaster prevention measures, meaning that potentially hazardous tsunamis (with wave heights above a certain level, for example, higher than 1.0 m near the Samcheok area) may occur without warning. In addition, tsunamis could reach the beaches of Gyeongpo, Mangsang, Maengbang, and Samcheok, which are popular summer tourist attractions, and Uljin Nuclear Power Station. However, the fault-parameter-based scenarios adopted in this study are not directly applicable to the national earthquake and tsunami forecasting system and the national disaster prevention plan because they estimate the worst-cases of tsunami threat of local tsunamis in the East Sea. Nevertheless, considering that tsunamis can lead to

large-scale disasters once generated, the potential risks must be considered in advance when building the national disaster prevention system with respect to the hazard presented by tsunamis. A detailed analysis of this issue is discussed below in **Section 4.3**

4.2 Quantitative Evaluation of Local Tsunami Hazard in the East Sea

As described above, the maximum runup heights of tsunamis that can be generated on the eastern coast were calculated, and these are presented in **Figure 10**. In general, even if a grid nesting technique is used to construct a precise grid during tsunami numerical modeling, the accuracy of tsunami reproduction is low

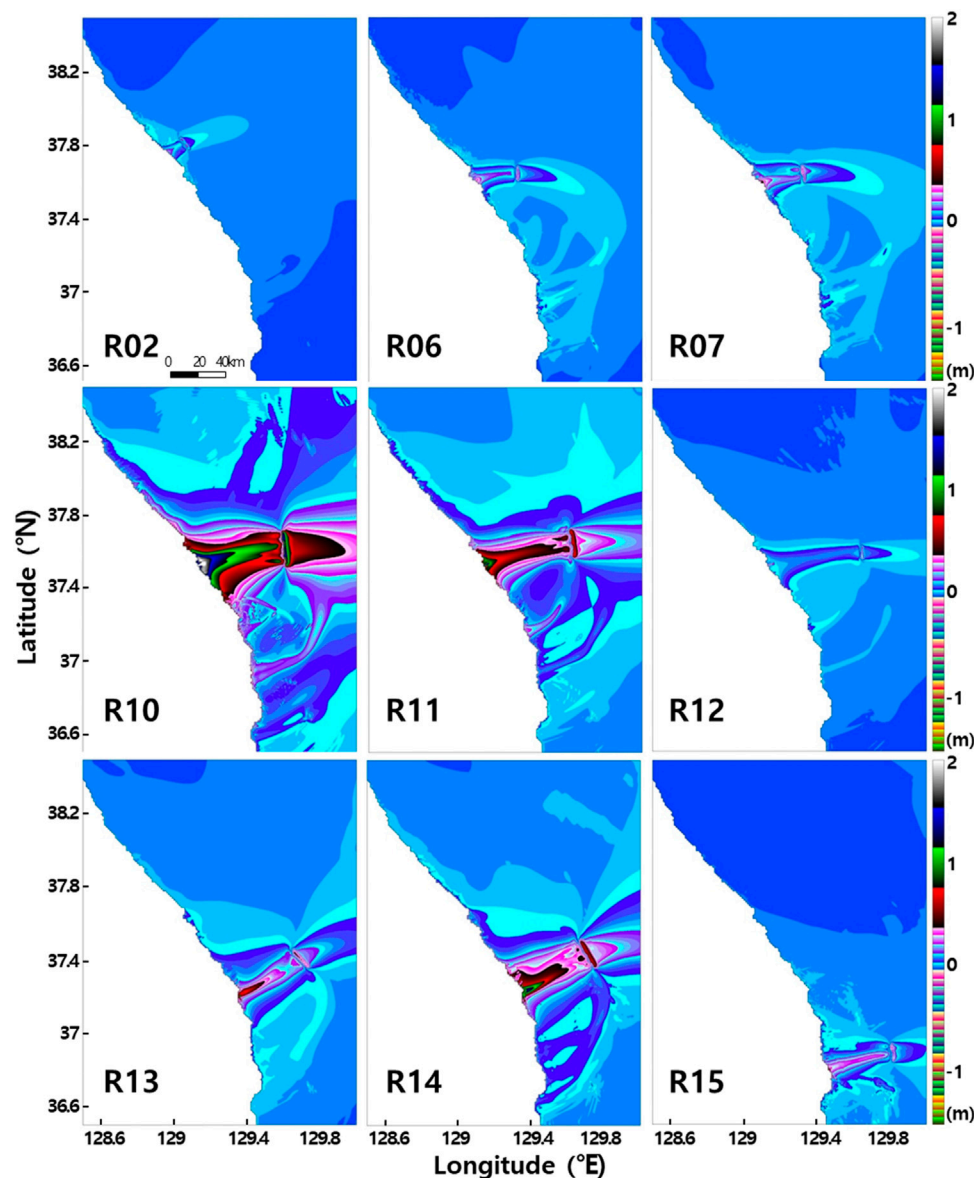


FIGURE 7 | Maximum wave height of tsunamis in the East Sea, estimated from numerical modeling for different scenarios (fault zones; Combination B).

in areas with shallow water depths and complicated bathymetry near the coast owing to the constant size of the computational grid. Calculation methods such as composing finer calculation grids near the coast are available to overcome this issue. However, such methods are time consuming and impractical to calculate for the entire peninsula. Alternatively, the Japan Meteorological Agency (JMA) applies Green's law to estimate tsunami wave heights in coastal waters with minor errors for the purpose of tsunami forecasting and warning. It has been shown that Green's law is valid only outside the source region (Fine et al., 2013; Sandanbata et al., 2018) and that tsunami runups calculated for tsunami sources outside of the source region, such as that of the 2011 Great East Japan Earthquake tsunami (which was located very close to the coastline of Japan) are very different from those

calculated using Green's law. In this study, potential local tsunamis originate offshore from the eastern coast of the Korean Peninsula, meaning that Green's law can be suitably applied to estimate the probable maximum runup of tsunamis. The JMA has applied Green's law to obtain the wave height at 1 m water depth and whose value is taken as the tsunami wave height at the coast (Mulia et al., 2020). This study estimated maximum tsunami runup heights along the studied eastern Korea coastline by following the method adopted by the JMA. The risk of tsunami for the studied coastline was analyzed using the values obtained.

Figure 11 presents the maximum tsunami runup heights calculated by applying Green's law to the numerical modeling results for the studied tsunami scenarios. "Combination A" in **Figure 11** is based on a combination of the mean value from the

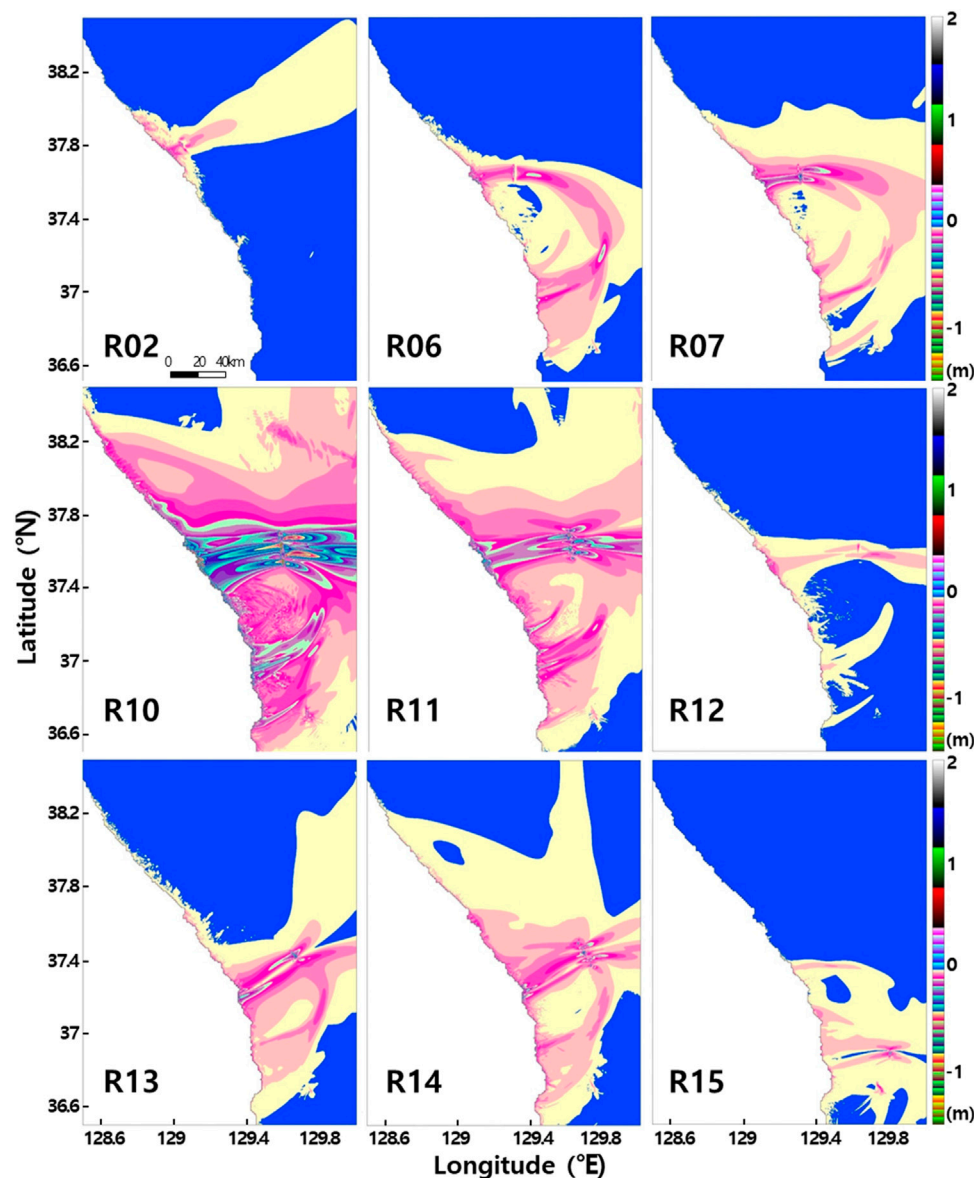


FIGURE 8 | Lowest elevation of tsunamis in the East Sea, estimated from numerical modeling for different scenarios (fault zones; Combination A).

empirical equations of Matsuda (1975) and Wells & Coppersmith (1994) and the slip angle value of the top fault zone (see **Table 1**). Results show that maximum runup heights exceeding 0.5 m in areas of 1 m water depth are widely observed. In particular, high runup heights of >2.0 m are estimated to occur across a wide area along the studied coastline for scenario R10. This wide area includes beaches, where approximately one million tourists visit on an average day during summer. Therefore, an early warning system and a plan for immediate evacuation of residents and tourists to safe locations are essential. In contrast, port infrastructure located on the eastern coast may be fairly safe with respect to the estimated tsunami wave heights, as they have ~3.0 m freeboards, but vessels inside the harbors may be damaged. Lynett P. et al. (2012) found that local tsunamis with the highest tsunami wave height less than 0.5 m can generate extreme

currents in harbors, causing economic loss, and tsunami-induced currents near the coast should be carefully considered in addition to tsunami wave heights when evaluating tsunami hazards.

“Combination B” in **Figure 11** is based on a combination of the mean slip angle value (see **Table 1**) of the tsunami-instigating fault zone and the amplified initial sea surface displacement due to an upward adjustment of fault zones along with the mean displacement value from five empirical equations (see **Table 3**). In contrast to the results from Combination A, maximum runup heights were estimated to exceed 1.5 m at a 1 m water depth for some areas. In particular, for scenarios R7, R10, and R11, runup heights were predicted to exceed 4.0 m, potentially inundating large areas and threatening human lives, property, and infrastructure along the eastern coast. Therefore, additional research into forecasting

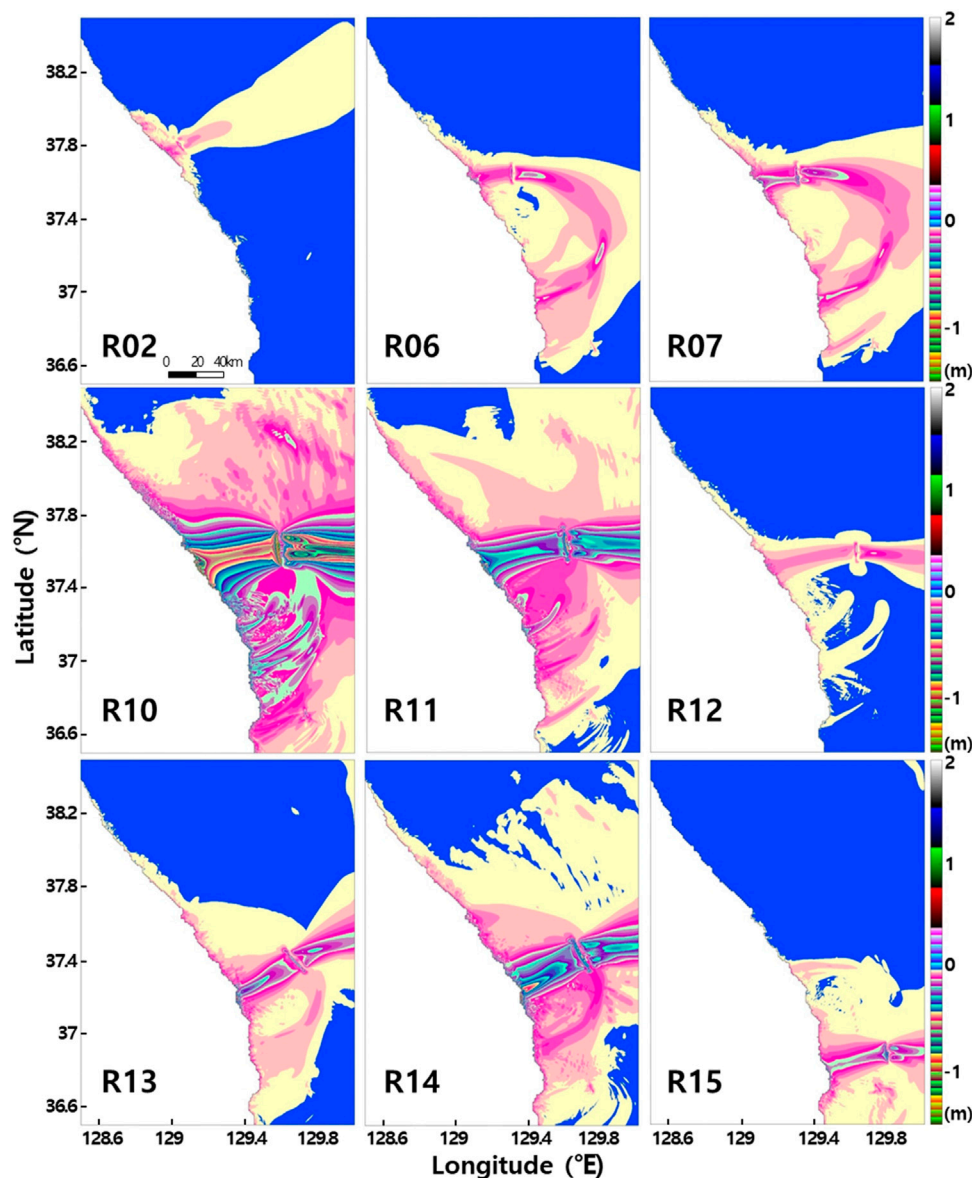


FIGURE 9 | Lowest elevation of tsunamis in the East Sea, estimated from numerical modeling for different scenarios (fault zones; Combination B).

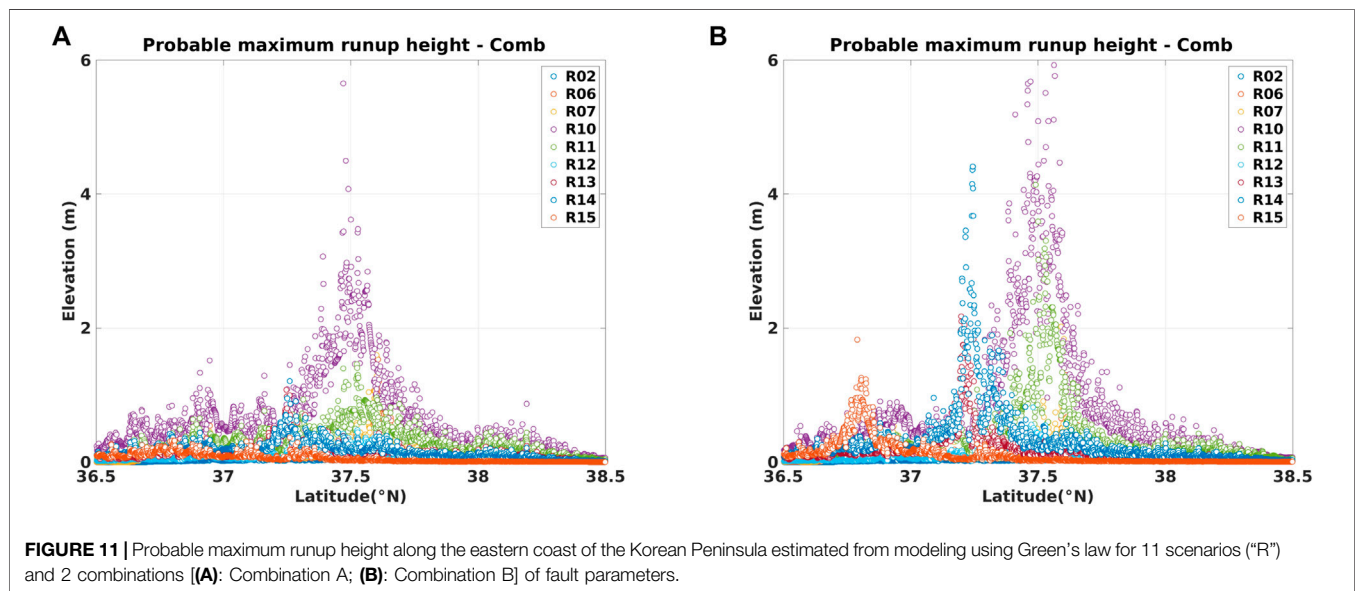
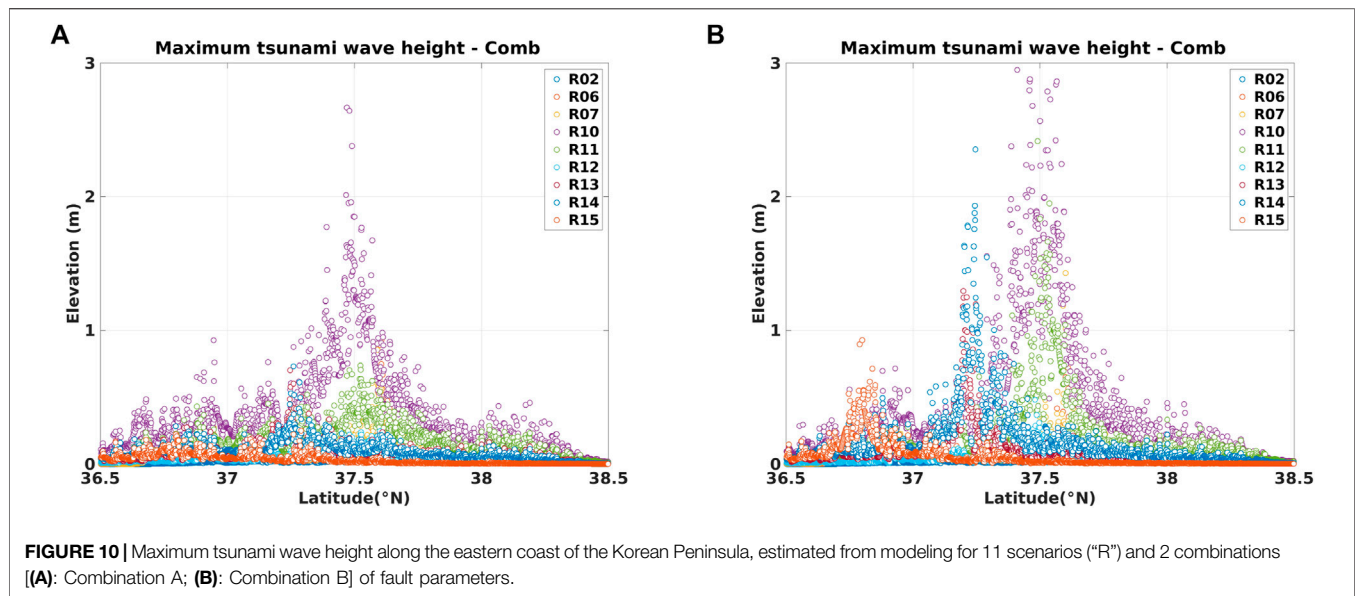
tsunamis and the propagation of tsunami energy for risk assessment of coastal areas is necessary, possibly implementing recently proposed methodologies, such as new the paradigm for mass, momentum, and energy of nearshore tsunamis developed by Kim and Son (2018, 2019).

4.3 Scenario-Based Assessment of the Potential Threat and Damage Caused by Local Tsunamis in the East Sea

The 2011 Great East Japan Earthquake tsunami was an extremely large tsunami with an estimated recurrence interval of ≥ 1000 years, and it caused damage estimated at 300 billion U.S. dollars (Daniell et al., 2011). The Japanese government

had developed its tsunami response system without considering such extremely large tsunamis in the possible range, meaning that unexpected levels and types of damage occurred, such as the inundation and meltdown of the Fukushima Nuclear Power Plant. South Korea and China were also affected by radiation derived from the nuclear accident. Japan has since entirely revised its national tsunami response system. Given the example of Japan, the threat posed by tsunamis to the eastern coastline of Korea must be properly quantified and a response system established with respect to the full range of estimated tsunami sizes.

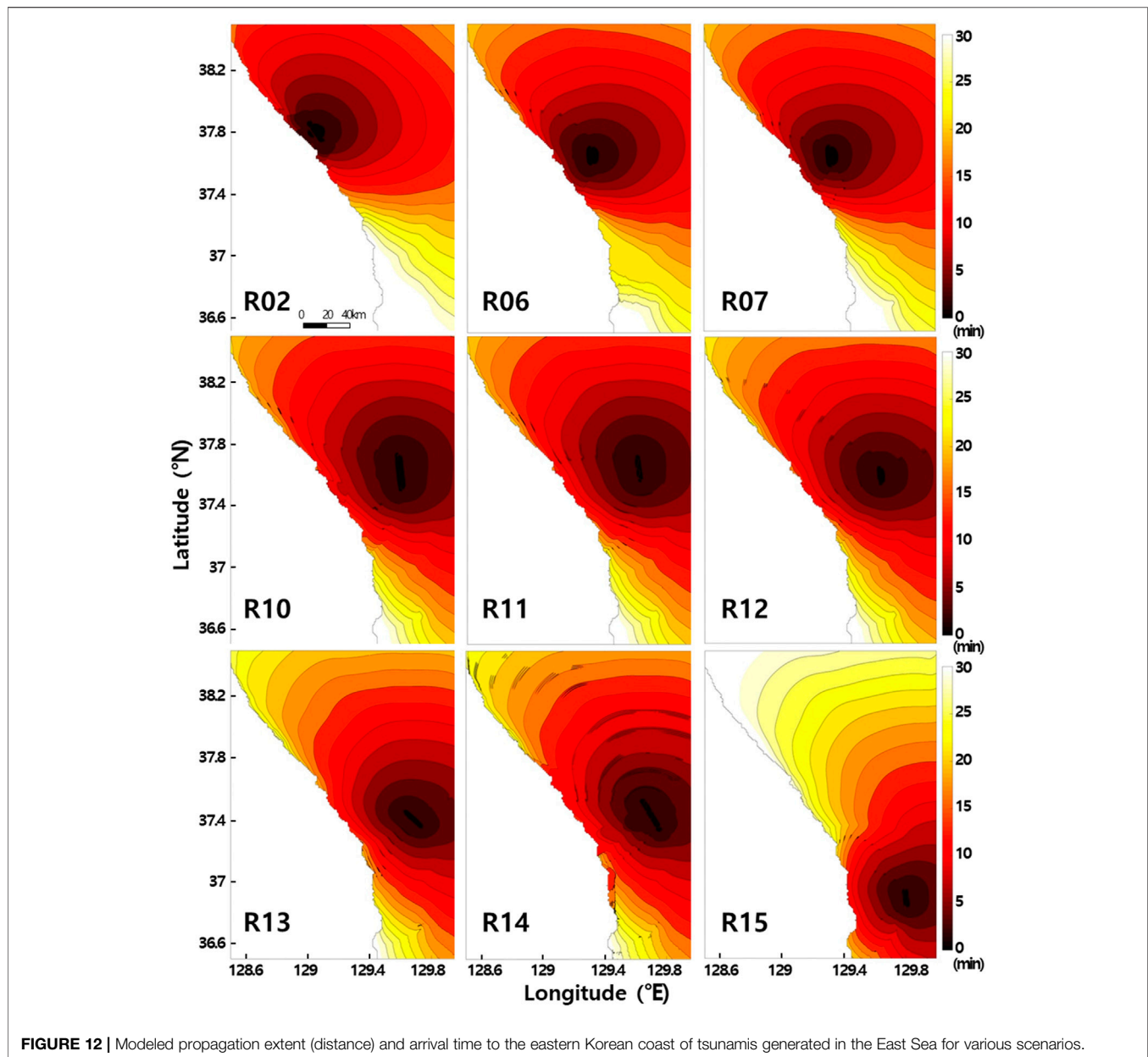
After numerical modeling of tsunami propagation in the East Sea according to each fault parameter scenario (Section 4.1), an index of tsunami intensity proposed by Boschetti and Ioualalen



(2021) was used to assess tsunami hazard along the eastern coast considering tsunami currents as well as tsunami wave heights. Lynett et al. (2014) first proposed the index to connect current speed of a tsunami with damage state and the index was divided into the six damage states, which were 0: no damage/impacts, 1: small buoys moved; 2: 1–2 docks/small boats damaged and/or large buoys moved; 3: moderate dock/boat damage (<25% of docks/vessels damaged) and/or midsized vessels off moorings; 4: major dock/boat damage (<50% of docks/vessels damaged) and/or large vessels off moorings; 5: extreme/complete damage (>50% of docks/vessels damaged). Boschetti and Ioualalen (2021) extended the Lynett et al.'s and integrated several approaches (Shuto, 1993; Graszek et al., 1999; Papadopoulos and Imamura, 2001; Misesa, 2012; Charvet et al., 2014) connecting the tsunami

magnitude to damages on structures and persons. They finally proposed the new intensity scale based on the maximum tsunami wave height and current speed [see Section 4, Figure 4 and Table 5 in Boschetti and Ioualalen (2021)].

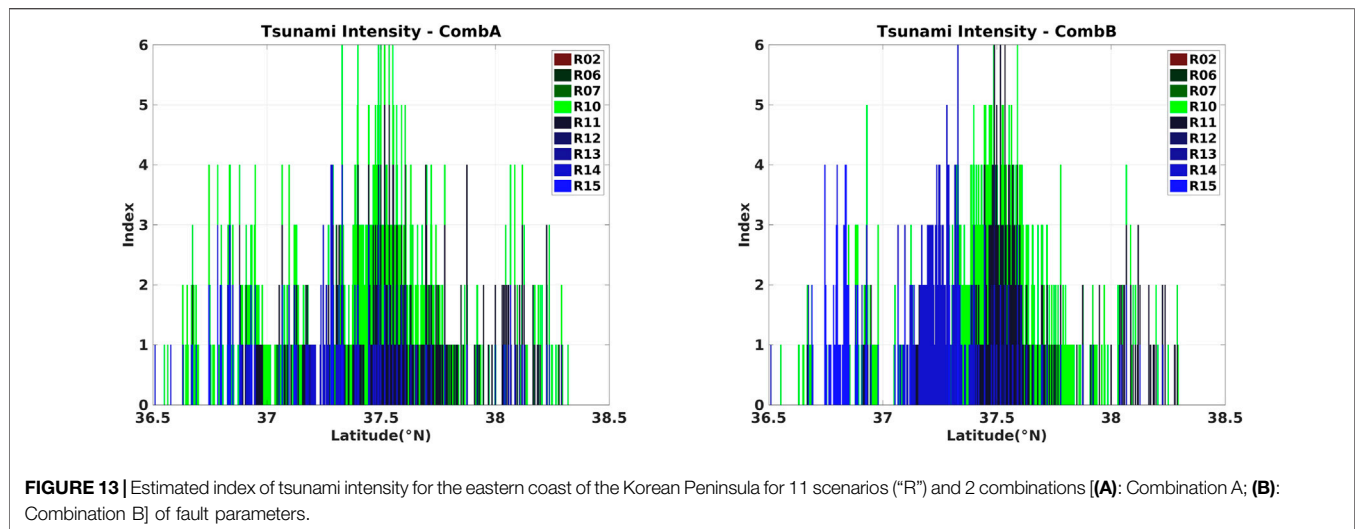
This type of assessment, which has large uncertainties and only broad constraints on data, usually demands a probabilistic approach (Geist and Parsons, 2006; Grezio et al., 2017; Satake et al., 2022). The present study, however, was originally motivated by historical evidence for possible tsunami events initiated in the East Sea and affecting the eastern coast of the Korean Peninsula. The possible tsunami events recorded in the Diaries of the Royal Secretariat contained anecdotal evidence that was interpreted in terms of the expected behavior of a tsunami, so the evidence was



validated qualitatively rather than involving detailed hindcasting. Therefore, an index of tsunami intensity, rather than probabilistic tsunami hazard analysis, was employed to evaluate tsunami threat along the Korean coast of the East Sea. **Figure 13** presents the estimated latitudinal distribution of the index of tsunami intensity calculated using combinations A and B. The fault-parameter scenario generating the most damage on the studied coast was R10 in both combinations, and the highest level of tsunami intensity observed along the coast was 6. In comparison with tsunami wave height, tsunami-induced currents produced smaller effects on tsunami intensity for both combinations, but they resulted in the higher values of tsunami intensity estimated for Combination B compared with Combination A. As a result,

a highest level of tsunami intensity of 6 was reached for scenarios R07, R10, and R11 in Combination B, whereas only R10 reached this value in Combination A.

An estimated runup height of >11.0 m could occur in a scenario R10, which could generate considerable damage at the coast. The fault-parameter scenarios examined in this study were generated based on past observational data, including seismic survey records, and it is concerned that excessive variables can be introduced for fault parameter scenarios. Few raised doubts on the realistic response and relevant research for the coastal waters of the Korean Peninsula, which had no risk of tsunami occurrence in the last hundreds of years. However, it is important to note that the Japanese government did not consider the 2011 Great East Japan



Earthquake tsunami as a possible scenario in their economic and political decision-making process, despite Japanese scientists being aware of the possibility of such large tsunami-causing earthquakes (Synolakis and Kanoglu, 2015). Furthermore, coastal events that can be regarded as local tsunamis in the East Sea have been recorded in the historical literature for various parts of the eastern coast of Korea. Underestimating the threat posed by tsunamis is a risk in terms of potential loss of human life and infrastructural and economic damage. The present study examined local tsunamis with the aim of better understanding their occurrence and impact as a basis for informing the development of a prediction and warning system and the establishment of mitigation measures. It should be noted that this study did not consider a fault parameter scenario in which simultaneous tsunamis were generated by simultaneously activated multiple fault zones, as was the case for the 2011 Great East Japan Earthquake tsunami. Such a large-magnitude-tsunami scenario for the eastern coast of Korea was considered to be immoderate although we estimated the most extreme conditions of local tsunamis based on past observational data, including seismic survey records.

5 CONCLUDING REMARKS

In this study, we assessed the possibility of a submarine earthquake occurring in the East Sea by examining historical records and investigating fault zones, and modeled the propagation of a potential local tsunami along the East Sea coast of the Korean Peninsula. Tsunami numerical modeling with different scenarios of fault parameters reproduced the features inferred from presumed tsunamis recorded in the historical documents, including the maximum runup height, which was consistent with the range interpreted from

historical records. The historical records and numerical modeling results from this study suggest that local tsunamis have occurred on the eastern seaboard of Korea in the past and are therefore likely to do so in the future. Our results should help inform tsunami forecasting, preparedness, and mitigation on the eastern coast of Korea, including the development of warning systems and the inclusion of tsunami hazards in the national disaster prevention system.

DATA AVAILABILITY STATEMENT

The original contributions presented in the study are included in the article/supplementary material, further inquiries can be directed to the corresponding author.

AUTHOR CONTRIBUTIONS

TH applied the methodology and drafted the manuscript; TH and K-HK critically revised the paper and supervised the study; JK, S-HY, D-WL, and J-SY provided suggestions on the results. All authors contributed to the article and approved the submitted version.

FUNDING

This work was funded by the Korea Meteorological Administration Research and Development Program under Grant KMI2022-00610 and the Basic Science Research Program through the National Research Foundation of Korea (NRF) funded by the Ministry of Science and ICT (NRF-2020R1A2C2011751).

REFERENCES

- Anderson, J. R. (1996). ACT: A Simple Theory of Complex Cognition. *Am. Psychol.* 51 (4), 355–365. doi:10.1037/0003-066x.51.4.355
- Bonilla, M. G., Villalobos, H. A., and Wallace, R. E. (1984). Exploratory Trench across the Pleasant Valley Fault, Nevada. *Prof. Pap. U.S. Geol. Surv.* 1274, 1–34.
- Boschetti, L., and Ioualalen, M. (2021). Integrated Tsunami Intensity Scale Based on Maxima of Tsunami Amplitude and Induced Current. *Nat. Hazards* 105 (1), 815–839. doi:10.1007/s11069-020-04338-5
- Butler, R., Stewart, G. S., and Kanamori, H. (1979). The July 27, 1976 Tangshan, China Earthquake—A Complex Sequence of Intraplate Events. *Bull. Seismol. Soc. Am.* 69 (1), 207–220. doi:10.1785/bssa0690010207
- Chai, M. F., Lau, T. L., and Majid, T. A. (2014). RETRACTED: Potential Impacts of the Brunei Slide Tsunami over East Malaysia and Brunei Darussalam. *Ocean. Eng.* 81, 69–76. doi:10.1016/j.oceaneng.2014.02.028
- Charvet, I., Suppasri, A., and Imamura, F. (2014). Empirical Fragility Analysis of Building Damage Caused by the 2011 Great East Japan Tsunami in Ishinomaki City Using Ordinal Regression, and Influence of Key Geographical Features. *Stoch. Environ. Res. Risk Assess.* 28, 1853–1867. doi:10.1007/s00477-014-0850-2
- Chiu, J.-M., and Kim, S. G. (2004). Estimation of Regional Seismic Hazard in the Korean Peninsula Using Historical Earthquake Data between A.D. 2 and 1995. *Bull. Seismol. Soc. Am.* 94, 269–284. doi:10.1785/0120010256
- Daniell, J. E., Khazai, B., Wenzel, F., and Vervaeck, A. (2011). The CATDAT Damaging Earthquakes Database. *Nat. Hazards Earth Syst. Sci.* 11 (8), 2235–2251. doi:10.5194/nhess-11-2235-2011
- Fine, I. V., Kulikov, E. A., and Cherniawsky, J. Y. (2013). Japan's 2011 Tsunami: Characteristics of Wave Propagation from Observations and Numerical Modelling. *Pure Appl. Geophys.* 170, 1295–1307. doi:10.1007/s00024-012-0555-8
- GEBCO Compilation Group (2021). *GEBCO 2021 Grid*. Berlin: GEBCO. doi:10.5285/a29c5465-b138-234d-e053-6c86abc040b9
- Geist, E. L., and Parsons, T. (2006). Probabilistic Analysis of Tsunami Hazards*. *Nat. Hazards* 37 (3), 277–314. doi:10.1007/s11069-005-4646-z
- Grasz, E., Roy, J. L., Garry, G., Guyot, P., and Hubert, T. (1999). *Plans de prévention des risques naturels (PPR): Risques d'inondation—Guide méthodologique*. Paris, Aubervilliers: La documentation Française.
- Grezio, A., Babeyko, A., Baptista, M. A., Behrens, J., Costa, A., Davies, G., Geist, E. L., Glimsdal, S., González, F. I., Griffin, J., Harbitz, C. B., LeVeque, R. J., Lorito, S., Løvholt, F., Omira, R., Mueller, C., Paris, R., Parsons, T., Polet, J., Power, W., Selva, J., Sørensen, M. B., and Thio, H. K. (2017). Probabilistic Tsunami Hazard Analysis: Multiple Sources and Global Applications. *Rev. Geophys.* 55 (4), 1158–1198. doi:10.1002/2017rg000579
- Ha, T., and Cho, Y.-S. (2015). Tsunami Propagation over Varying Water Depths. *Ocean. Eng.* 101, 67–77. doi:10.1016/j.oceaneng.2015.04.006
- Han, M., Kim, H.-J., Kang, S. Y., Kim, K.-H., Yoon, S. H., and Kyung, J. B. (2019). Detection of Microearthquakes and Identification of Their Causative Structures in the Eastern Offshore Region of South Korea. *Tectonophysics* 750, 36–44.
- Johnston, A. C., and Schweig, E. S. (1996). The Enigma of the New Madrid Earthquakes of 1811–1812. *Annu. Rev. Earth Planet. Sci.* 24, 339–384. doi:10.1146/annurev.earth.24.1.339
- KIGAM (2016). *Marine Geological and Geophysical Mapping of the Korean Seas*. Daejeon, South Korea: Ministry of Science, ICT and Future Planning.
- KIGAM (2010). *Study on the Coastal Geohazard Factors Analysis*. Daejeon, South Korea: Ministry of Land, Infrastructure, and Transport.
- Kim, C. S. (1982). Submarine Geology of Continental Margin of the East Sea, Korea. *Min. Geol.* 15, 65–88.
- Kim, D.-H., and Son, S. (2019). Role of Shelf Geometry and Wave Breaking in Single N-type Tsunami Runup under Geophysical-Scale. *Ocean. Model.* 138, 13–22. doi:10.1016/j.ocemod.2019.05.001
- Kim, D. H., and Son, S. (2018). Lagrangian-like Volume Tracking Paradigm for Mass, Momentum and Energy of Nearshore Tsunamis and Damping Mechanism. *Sci. Rep.* 8 (1), 1–11. doi:10.1038/s41598-018-32439-6
- Kim, K.-H., Kang, T.-S., Rhie, J., Kim, Y., Park, Y., Kang, S. Y., et al. (2016). The 12 September 2016 Gyeongju Earthquakes: 2. Temporary Seismic Network for Monitoring Aftershocks. *Geosci. J.* 20, 753–757. doi:10.1007/s12303-016-0034-9
- Kim, K.-H., Ree, J.-H., Kim, Y., Kim, S., Kang, S. Y., and Seo, W. (2018b). Assessing whether the 2017 M W 5.4 Pohang Earthquake in South Korea Was an Induced Event. *Science* 360, 1007–1009. doi:10.1126/science.aat6081
- Kim, K. H., Kim, J., Han, M., Kang, S. Y., Son, M., Kang, T. S., et al. (2018a). Deep Fault Plane Revealed by High-Precision Locations of Early Aftershocks Following the 12 September 2016 M L 5.8 Gyeongju, Korea, Earthquake. *Bull. Seismol. Soc. Am.* 108, 517–523. doi:10.1785/0120170104
- Kim, K. H., Yoon, S. H., Kyung, J. B., Seo, M. C., Kim, J. K., and Ha, T. (2018c). *Seismicity in the West Sea and the Evaluation of Localized Tsunami Potential in the East Sea*. Seoul: Korea Meteorological Administration.
- Kyung, J. B., Jung, M. K., Baek, J. J., Im, Y. J., and Lee, K. (2010). *Historic Earthquake Catalog in the Korea Peninsula*. Seoul: Korea Meteorological Administration, 475.
- Lee, E., Jung, T., Kim, J.-C., and Shin, S. (2019a). A Study of the Optimal Deployment of Tsunami Observation Instruments in Korea. *J. Ocean. Eng. Technol.* 33 (6), 607–614. doi:10.26748/ksoe.2019.100
- Lee, K., and Yang, W. S. (2006). Historical Seismicity of Korea. *Bull. Seismol. Soc. Am.* 96, 846–855. doi:10.1785/0120050050
- Lee, W.-D., Kim, J.-O., and Hur, D.-S. (2019b). Effects of Waveform Distribution of Tsunami-like Solitary Wave on Run-Up on Impermeable Slope. *J. Ocean. Eng. Technol.* 33 (1), 76–84. doi:10.26748/ksoe.2018.059
- Lynett, P. J., Borrero, J. C., Weiss, R., Son, S., Greer, D., and Renteria, W. (2012a). Observations and Modeling of Tsunami-Induced Currents in Ports and Harbors. *Earth Planet. Sci. Lett.* 327–328, 68–74. doi:10.1016/j.epsl.2012.02.002
- Lynett, P. J., Borrero, J., Son, S., Wilson, R., and Miller, K. (2014). Assessment of the Tsunami-Induced Current Hazard. *Geophys. Res. Lett.* 41 (6), 2048–2055. doi:10.1002/2013gl058680
- Lynett, P., Weiss, R., Renteria, W., De La Torre Morales, G., Son, S., Arcos, M. E. M., et al. (2012b). Coastal Impacts of the March 11th Tohoku, Japan Tsunami in the Galapagos Islands. *Pure Appl. Geophys.* 170, 1189–1206. doi:10.1007/s00024-012-0568-3
- Matsuda, T. (1975). Magnitude and Recurrence Interval of Earthquakes from a Fault. *Jssj* 28, 269–283. doi:10.4294/zisin1948.28.3_269
- Ministry of Public Safety and Security (2017). *Earthquake Whitepaper*. Seoul, Korea: Ministry of Interior and Safety.
- Ministry of the Interior and Safety (2018). *Pohang Earthquake Whitepaper*. Seoul, Korea: Ministry of Interior and Safety.
- Misea, j. (2012). “Plan de prévention des risques naturels d'inondation: Bassin versant de l'Etang de Thau, Commune de Villeveyrac,” in *Direction Départementale des Territoires et de la Mer—Service Eau et Risques* (Paris, Aubervilliers: Préfecture de l'Hérault).
- Mulia, I. E., Ishibe, T., Satake, K., Gusman, A. R., and Murotani, S. (2020). Regional Probabilistic Tsunami Hazard Assessment Associated with Active Faults along the Eastern Margin of the Sea of Japan. *Earth Planets Space* 72 (1), 1–15. doi:10.1186/s40623-020-01256-5
- Okada, Y. (1985). Surface Deformation Due to Shear and Tensile Faults in a Half-Space. *Bull. Seismol. Soc. Am.* 75 (4), 1135–1154. doi:10.1785/bssa0750041135
- Papadopoulos, G. A., and Imamura, F. (2001). “A Proposal for a New Tsunami Intensity Scale,” in *Int. Tsunami Symp. 2001 Proc.* 7–9 Aug. 2001 (Seattle, Washington: IOC/UNESCO), 569–577.
- Park, S.-C., and Mori, J. (2005). Source Parameters of the May 29, 2004 South Korea Earthquake (M L 5.2). *Earth, Planets Space* 57, 471–475.
- Park, S.-C., You, S., Choi, M., and Lee, H.-W. (2020). Application of Tsunami Scenario Database and Numerical Simulation to Tsunami Warning and Notification Process. *Korea Soc. Coast. Disaster Prev.* 7 (1), 11–20. doi:10.20481/kscdp.2020.7.1.11
- Sandanbata, O., Watada, S., Satake, K., Fukao, Y., Sugioka, H., Ito, A., et al. (2018). Ray Tracing for Dispersive Tsunamis and Source Amplitude Estimation Based on Green's Law: Application to the 2015 Volcanic Tsunami Earthquake Near Torishima, South of Japan. *Pure Appl. Geophys.* 175, 1371–1385. doi:10.1007/s00024-017-1746-0
- Satake, K., Ishibe, T., Murotani, S., Mulia, I. E., and Gusman, A. R. (2022). Effects of Uncertainty in Fault Parameters on Deterministic Tsunami Hazard Assessment: Examples for Active Faults along the Eastern Margin of the Sea of Japan. *Earth Planets Space* 74 (1), 1–20. doi:10.1186/s40623-022-01594-6
- Schluter, H. V., and Chun, W. C. (1974). Seismic Survey of the East Coast of Korea. *U. N. ECAFE/CCOP Tech. Bull.* 8, 1–16.

- Shuto, N. (1993). "Tsunami Intensity and Disasters," in *Tsunamis in the World*. Editor S. Tinti (Dordrecht: Kluwer Academic Publishers), 197–216. doi:10.1007/978-94-017-3620-6_15
- Slemmons, D. B. (1988). "Crustal Extension: Continental Extensional Tectonics," in *Published for the Geological Society by Blackwell Scientific*. Editors M. P. Coward, J. F. Dewey, and P. L. Hancock (Palo Alto, CA: Geological Society Special Publication). doi:10.1126/science.239.4844.1185.a
- Son, S., Lynett, P. J., and Kim, D.-H. (2011). Nested and Multi-Physics Modeling of Tsunami Evolution from Generation to Inundation. *Ocean. Model.* 38 (1-2), 96–113. doi:10.1016/j.ocemod.2011.02.007
- Synolakis, C., and K anođlu, U. (2015). The Fukushima Accident Was Preventable. *Phil. Trans. R. Soc. A* 373, 20140379. doi:10.1098/rsta.2014.0379
- Vakov, A. V. (1996). Relationships between Earthquake Magnitude, Source Geometry and Slip Mechanism. *Tectonophysics* 261 (1-3), 97–113. doi:10.1016/0040-1951(96)82672-2
- Wang, X., and Liu, P. L.-F. (2011). An Explicit Finite Difference Model for Simulating Weakly Nonlinear and Weakly Dispersive Waves over Slowly Varying Water Depth. *Coast. Eng.* 58, 173–183. doi:10.1016/j.coastaleng.2010.09.008
- Wang, X. (2009). *User Manual for COMCOT Version 1.7*. New Zealand: Institute of Geological & Nuclear Science.
- Wells, D. L., and Coppersmith, K. J. (1994). New Empirical Relationships Among Magnitude, Rupture Length, Rupture Width, Rupture Area, and Surface Displacement. *Bull. Seismol. Soc. Am.* 84 (4), 974–1002.
- Wessel, P., Smith, W. H. F., Scharroo, R., Luis, J., and Wobbe, F. (1998). Generic Mapping Tools: Improved Version Released. *EOS Trans. Amer. Geophys. U.* 94 (45), 409–410.
- Wijetunge, J. J. (2012). Nearshore Tsunami Amplitudes off Sri Lanka Due to Probable Worst-Case Seismic Scenarios in the Indian Ocean. *Coast. Eng.* 64, 47–56. doi:10.1016/j.coastaleng.2012.02.005
- Yoo, S. C., Mun, J. Y., Park, W., Seo, G. H., Gwon, S. J., and Heo, R. (2019). Development of Bathymetric Data for Ocean Numerical Model Using Sea-Floor Topography Data: BADA ver.1. *J. Korean Soc. Coast Ocean. Eng.* 31 (3), 146–157. doi:10.9765/kscoe.2019.31.3.146
- Yoon, S.-H., Kim, G. B., Joe, Y. J., Koh, C. S., and Kwon, Y. K. (2015). Origin and Evolution of Geologic Basement in the Korean Continental Margin of East Sea, Based on the Analysis of Seismic Reflection Profiles. *jgsk* 51 (1), 37–52. doi:10.14770/jgsk.2015.51.1.37
- Yoon, S. H. (1994). *The Eastern Continental Margin of Korea: Seismic Stratigraphy, Geologic Structure and Tectonic Evolution*. Seoul: Seoul National University. Ph.D. thesis.

Conflict of Interest: JSY is employed by the Korea Rural Community Corporation.

The remaining authors declare that the research was conducted in the absence of any commercial or financial relationships that could be construed as a potential conflict of interest.

Publisher's Note: All claims expressed in this article are solely those of the authors and do not necessarily represent those of their affiliated organizations, or those of the publisher, the editors and the reviewers. Any product that may be evaluated in this article, or claim that may be made by its manufacturer, is not guaranteed or endorsed by the publisher.

Copyright © 2022 Ha, Yoon, Kyung, Yoon, Lee and Kim. This is an open-access article distributed under the terms of the Creative Commons Attribution License (CC BY). The use, distribution or reproduction in other forums is permitted, provided the original author(s) and the copyright owner(s) are credited and that the original publication in this journal is cited, in accordance with accepted academic practice. No use, distribution or reproduction is permitted which does not comply with these terms.